ACSNANO

www.acsnano.org

ARTICLE

Collective Nanoparticle Dynamics Associated with Bridging Network Formation in Model Polymer Nanocomposites

Benjamin M. Yavitt, Daniel Salatto, Yuxing Zhou, Zhixing Huang, Maya Endoh, Lutz Wiegart, Vera Bocharova, Alexander E. Ribbe, Alexei P. Sokolov,* Kenneth S. Schweizer,* and Tadanori Koga*

Cite This: *ACS Nano* 2021, 15, 11501−11513

Read Online

ACCESS | Metrics & More | Article Recommendations | Supporting Information

ABSTRACT: **The addition of nanoparticles (NPs) to polymers is a powerful method to improve the mechanical and other properties of macromolecular materials. Such hybrid polymer−particle systems are also rich in fundamental soft matter physics. Among several factors contributing to mechanical reinforcement, a polymer-mediated NP network is considered to be the most important in polymer nanocomposites (PNCs). Here, we present an integrated experimental−theoretical study of the collective NP dynamics in model PNCs using X-ray photon correlation spectroscopy and microscopic statistical mechanics theory. Silica NPs dispersed in unentangled or entangled poly(2-vinylpyridine) matrices over a range of NP loadings are used. Static collective structure factors of the NP subsystems at temperatures above the bulk glass transition temperature reveal the formation of a network-like microstructure *via* polymer-mediated bridges at high NP loadings above the percolation threshold. The NP collective relaxation times are up to 3 orders of magnitude longer than the self-diffusion limit of isolated NPs and display a rich dependence with observation wavevector and NP loading. A mode-coupling theory dynamical analysis that incorporates the static polymer-mediated bridging structure and collective motions of NPs is performed. It captures well both the observed scattering wavevector and NP loading dependences of the collective NP dynamics in the unentangled polymer matrix, with modest quantitative deviations emerging for the entangled PNC samples. Additionally, we identify an unusual and weak temperature dependence of collective NP dynamics, in qualitative contrast with the mechanical response. Hence, the present study has revealed key aspects of the collective motions of NPs connected by polymer bridges in contact with a viscous adsorbing polymer medium and identifies some outstanding remaining challenges for the theoretical understanding of these complex soft materials.**

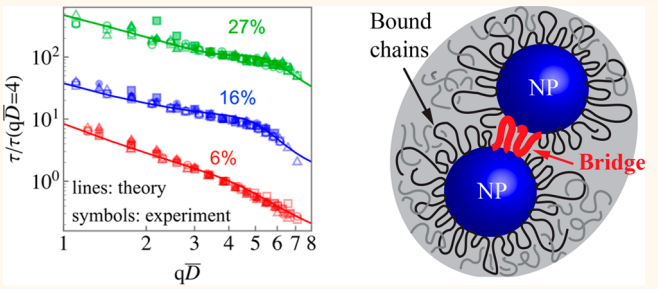

KEYWORDS: *polymer nanocomposites, collective nanoparticle dynamics, polymer bridges, x-ray photon correlation spectroscopy, mode-coupling theory, PRISM theory*

Polymer nanocomposites (PNCs) have been of considerable interest to both the materials science and soft matter communities for the last several decades.[1−3] The basic problem of rigid nanoscopic objects immersed in a highly viscoelastic matrix of flexible chain molecules is rich in soft matter physics and relevant in varied biophysical contexts. In the materials science and engineering arena, various property improvements such as increased modulus, stiffness, electrical conductivity, or magnetic susceptibility[4,5] are obtained when nanoparticles (NPs) are added to dense polymer melts or thermoplastics. Of particular interest is improving mechanical properties, where small additions of NPs to a polymer matrix result in several orders of magnitude increase in modulus.[6−8] The wide variety of available NPs and polymer matrices leads to a large parameter space for future material design.

There is growing evidence to suggest that mechanical reinforcement in PNCs occurs when NPs bridged by polymer chains adsorbed on NP surfaces form percolating structures over large length scales.[9−12] As proposed initially by Stickney and Falb,[13] a "bound polymer layer (BPL)" is a polymer layer that is stabilized around the NP surface *via* cohesive attractive interactions. The consensus is that the thicknesses of the BPL

Received: February 10, 2021
Accepted: June 10, 2021
Published: June 15, 2021

https://doi.org/10.1021/acsnano.1c01283
ACS Nano 2021, 15, 11501−11513

in various PNCs are commensurate with the radius of gyration (R_g) of adsorbed polymer chains[14−22] (unless the distance to another interface is smaller than R_g). At a high NP volume fraction or loading (ϕ) typically required for commercial applications, the interparticle separation distance (ID)[23,24] between neighboring NPs decreases and chain confinement induced by neighboring NPs emerges.[25,26] At large enough interfacial polymer−NP attraction, the discrete BPL becomes thermodynamically disfavored, and relatively *tight* polymer-mediated bridges between neighboring NPs emerge, leading to a network-like microstructure[27] that reinforces the PNCs as a large-scale skeleton.[28] The formation of a percolating NP network has been reported based on mechanical property experiments[11,12,29−31] or structural characterization (*i.e.*, mass fractal structures) using X-ray/neutron scattering[32] or transmission electron microscopy.[33] However, much less is known about the dynamics of the NP network in PNCs due to the lack of experimental methods capable of providing direct dynamical information at the suitable length and time scales. Hence, a comprehensive correlation among the structure, dynamics, and property enhancement in PNCs remains an unsolved challenge.

In this article, we study the collective NP dynamics in PNCs using X-ray photon correlation spectroscopy (XPCS) which can probe time scales comparable to those measured in shear rheology, but in a spatially resolved manner over microscopic length scales from 10s to 100s of nm. Spherical silica (SiO_2, radius ≈10 nm) NPs are added to monodisperse poly(2-vinylpyridine) (P2VP) melts with two different molecular weights (M_w = 9 and 38 kg/mol; the entanglement molecular weight of P2VP is about 18 kg/mol)[18] as a model PNC. A series of PNCs with different NP loadings (ϕ = 0.01, 0.06, 0.16, and 0.27) were prepared, and the collective structures and dynamics of NPs are investigated at temperatures far above the bulk glass transition temperature ($T_g \approx 100$ °C for M_w = 38 kg/mol and ≈90 °C for M_w = 9 kg/mol).[8] The choice of weakly entangled M_w is motivated by previous experimental results where the mechanical enhancement of highly loaded SiO_2/P2VP PNCs was improved the most at M_w = 38 kg/mol among the values of polymer M_w studied that ranged from 9 kg/mol to 404 kg/mol.[8] In addition, we employ in a predictive manner the dynamical mode-coupling theory (MCT) that incorporates the effect of bridging microstructure on the collective NP dynamics over a wide range of length and time scales. The following results stand out: (i) long-range concentration fluctuations associated with the emergence of a polymer bridged NP network are observed in the static structure factors of the PNCs above a viscoelastic gel point ($\phi_c \approx 0.16$); (ii) the rich scattering wavevector (q) dependence of the NP collective relaxation times is established as a function of filler loading; (iii) the NP collective relaxation times are categorized into the two regimes: short time self-diffusion dominant and collective dynamics dominant; (iv) the MCT analysis predicts the q and ϕ dependence of the NP collective relaxation times well for the unentangled PNCs, while modest deviations from experiments for the loading dependence emerge for the entangled PNCs; (v) the temperature dependence of the NP collective relaxation times are very unusual, becoming weaker as a stronger network is formed with increasing ϕ, which is the opposite trend of the mechanical response of the PNCs. Hence, the present study using the model PNCs reveals the correlation/decoupling between the microscopic structural/dynamical properties and relevant macroscopic properties, which will be beneficial for many other PNCs that are expected to be integral components of future polymer-based applications.[2] Moreover, our findings illuminate rich and complex physics and material design problems in PNCs where neighboring NPs connected by bridges control the mechanical properties.[28]

RESULTS AND DISCUSSION

Dynamic Mechanical Analysis. Before we discuss the collective structure and dynamics of NPs at the microscopic scale, we consider the macroscopic mechanical properties of the PNCs, identifying the emergence of bridged NP percolation with increasing NP loadings.[11,12,17,30] SiO_2 NPs with an average radius of R_N = 9.1 or 11.8 nm were dispersed in a P2VP matrix with molecular weight M_w = 9 and 38 kg/mol (we hereafter assign them as P2VP9k and P2VP38k, respectively). NPs with R_N = 9.1 nm were used with the P2VP38k sample, while R_N = 11.8 nm was used with the P2VP9k sample. A series of PNCs with increasing volume fraction of NPs (ϕ = 0.01, 0.06, 0.16, and 0.27) were prepared by dropcasting and subsequent solvent evaporation.[27] We performed rheology experiments on the P2VP9K and P2VP38k series from 120−176 °C at approximately 10 °C increments.

Dynamic master curves of the shifted frequency-dependent viscoelastic moduli, $G'(\omega)$ and $G''(\omega)$, for the P2VP38k series constructed using time−temperature superposition are plotted in Figure 1a and subsequently shifted by an additional vertical shift factor (b_T) for clarity. Dynamic master curves of the

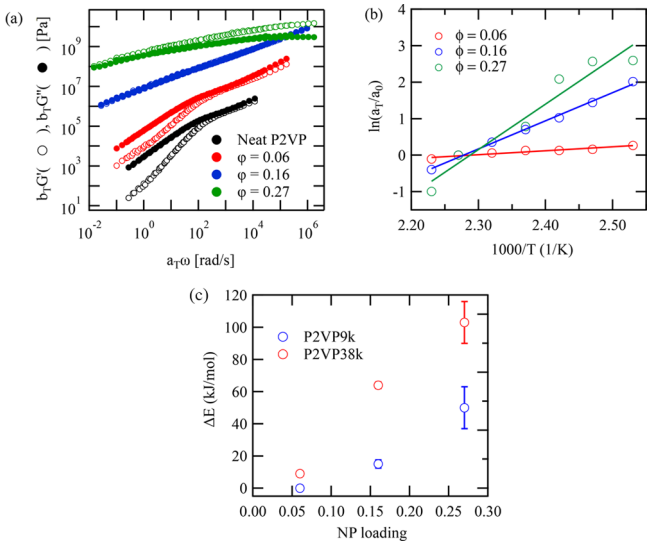

Figure 1. (a) Dynamic viscoelastic master curves $G'(\omega)$ and $G''(\omega)$ for the P2VP38k series generated by shifting small amplitude frequency sweeps according to time−temperature superposition (the reference temperature was set to 167 °C). $G'(\omega)$ and $G''(\omega)$ vertically shifted by an additional shift factor b_T for clarity: b_T = 10, 100, and 1,000 for ϕ = 0.06, 0.16, and 0.27, respectively. Time−temperature shift factors for the PNCs and the neat polymer used in the construction of dynamic master curves are shown in Figure S1a. (b) Shift factor (a_T) for the P2VP38k series normalized by the shift factor for the neat 38k melt (a_0) as a function of inverse temperature. The solid lines show the best-fits of eq 1 to the PNC data to calculate the extra activation energy (ΔE). (c) NP loading dependence of ΔE for the P2VP9k and P2VP38k series.

https://doi.org/10.1021/acsnano.1c01283
ACS Nano 2021, 15, 11501−11513

shifted $G'(\omega)$ and $G''(\omega)$ for the P2VP9k series and the horizontal shift factors (a_T) used for master curve generation are summarized in Figure S1 in Supporting Information (SI). The neat P2VP matrices were also characterized. We note that the rheological properties of the dilute PNC (ϕ = 0.01) samples are indistinguishable from the bulk P2VP matrices. The neat polymer matrix is a viscoelastic liquid, exhibiting the terminal flow regime scaling of $G' \sim \omega^2$ and $G'' \sim \omega^1$ at low ω. In the high ω limit, $G'' > G'$. A strong entanglement plateau is not observed, as the number of entanglements per chain is low for the 38K sample and absent for the 9K sample. At ϕ = 0.06, the shape of the master curve begins to adopt a nonpure-melt form where the time scales become extended and the low ω scaling changes to $G' \sim G'' \sim \omega^1$. The temperature dependence of the shift factors also begins to deviate from the bulk. A drastic change in the viscoelastic response is observed at ϕ = 0.16, where G' and G'' scale with an identical power law in frequency, per a rheological gel point.[34] At ϕ = 0.27, $G'(\omega) > G''(\omega)$ is evidenced across all accessible frequencies, indicating a transition to an elastically dominating behavior over accessible time scales. It should be noted that a similar ϕ dependence of the rheological properties (including the onset of gelation and features of solidification) for a SiO_2/P2VP system of comparable D and higher M_w was previously reported.[17] Hence, the rheology confirms that the PNCs do not flow on the experimental time scale from the macroscopic point of view at sufficiently high loading of NPs.

It is expected that the dynamics of the polymer bridging induced network is mainly controlled by the attachment−detachment process of adsorbed and confined polymers that connect the surfaces of two or more NPs.[35] According to a previous phenomenological model analysis,[36] the relaxation time of such chains (or the collection of segments that define the bridge) (τ_{ad}) is expressed as $\tau_{ad} \approx \mu(T)\exp(\Delta E/RT)$. A simple interpretation of ΔE is it reflects the activation energy for bridging polymer desorption per chain, and $\mu(T)$ and R are a temperature-dependent numerical constant and the gas constant, respectively. Motivated by such concepts, Cheng and co-workers[37] demonstrated that the shift factors of SiO_2 filled PNCs from oscillatory shear rheology follow:

$$a_T = a_0(T)\exp(\Delta E/RT - \Delta E/RT_{ref}) \quad (1)$$

where T_{ref} is the reference temperature and $a_0(T)$ is the dielectric shift factor which in the PNC was essentially identical to that in the pure polymer melt. The Boltzmann factor is meant to model in a simple manner the dissociation or dynamical breakup of the local structure associated with NP-polymer bridges which controls the lower frequency rheological properties of the PNCs. The ΔE values for the P2VP9k and P2VP38k series obtained from the best-fits of eq 1 to the experimental data (indicated by the solid lines in Figure 1b (P2VP38k) and Figure S1d (P2VP9k)) are summarized in Figure 1c. The magnitudes of ΔE for the P2VP38k samples are ≈60 kJ/mol and ≈100 kJ/mol at ϕ = 0.16 and ϕ = 0.27, respectively.

These activation energies reflect the cost to dynamically reorganize ("statistically break") the polymer-NP bridges in the PNCs, a process that plays a central role in the low-frequency rheology. Given the lack of a terminal flow regime in most of our PNCs, such polymer-mediated NP bridges are presumably not relaxed on the experimental time scale, as argued by Kumar and Colby[30] and explicitly incorporated in their sol−gel percolation modeling of the viscoelasticity of SiO_2-P2VP nanocomposites. This is important to keep in mind when considering the XPCS data (shown below) which probes time scales that are *not* longer than in the rheological measurements.

For the P2VP9k series, the ΔE activation energies are significantly smaller than those for the P2VP38k series at the same NP loadings (Figure 1c). There are many possible origins for this trend, but a model-independent interpretation is it reflects weaker interfacial cohesion of the bridging polymer segments and NPs for the low M_w sample. Mechanistically, this could involve equation of state effects (polymer melt density increases with M_w at lower degrees of polymerization), differences in P2VP local chain stiffness with M_w (influences packing), and/or larger scale issues associated with the ratio R_g/R_N or confinement parameter, ID. Resolving the mechanism is not important for the key results we present below.

Collective NP Structure Factors. We next study the microscopic static collective structure of the NPs in the PNCs. The interesting question is how polymers reorganize the NP microstructure as a function of length scale, loading, and polymer M_w. Such microstructural effects are expected to significantly impact the collective NP motions probed by XPCS.

The statistical NP microstructures are obtained *via* the time-integrated radial averaging of the small-angle X-ray scatting (SAXS) intensity $I(q)$ from XPCS experiments, where the wavevector $q = 4\pi\sin(\theta)/\lambda$ with 2θ the scattering angle in a small angle geometry and λ the X-ray wavelength. Representative SAXS spectra for the P2VP38k series at a temperature of 180 °C are presented in Figure S2. The measured $I(q)$ for the dilute sample (ϕ = 0.01) was used to calculate the NP form factor $P(q)$. The details have been described elsewhere.[27] The NP collective static structure factor $S(q)$ was then calculated by dividing $I(q)$ by the single NP form factor (*i.e.*, $S(q) = I(q)/P(q)$). The results are plotted as a function of dimensionless wavevector qD (where D is the mean particle diameter) in Figure 2 for each M_w series of PNCs. It is clear that the primary (cage) peak position q^* of $S(q)$, which is crudely related to an average interparticle spacing (d_t), increases with increasing ϕ, as does the intensity of the cage peak, $S(q^*)$, revealing the expected trends of denser and more correlated local NP

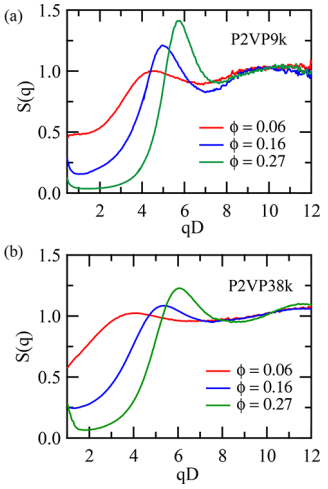

Figure 2. Structure factor $S(q)$ calculated according to SAXS intensities for each PNC sample: (a) P2VP9k and (b) P2VP38k at 180 °C. The *x*-axis is scaled with respect to the NP mean diameter (D).

https://doi.org/10.1021/acsnano.1c01283
ACS Nano 2021, 15, 11501−11513

packing as NP loading grows. As previously reported for the P2VP38k series,[27] we confirmed that the interparticle distance for the P2VP9k series remains unchanged with temperature over the very narrow temperature range explored in this study.

Another important feature of $S(q)$ is an upturn that emerges at scattering wavevectors well below the cage peak, $q < q^*$ (especially at $qD < 1$). As shown in Figure 2, the upturn is identified at $\phi = 0.16$ and 0.27 for both series. Based on the polymer reference interaction site model (PRISM) integral equation theory, we recently demonstrated that the upturn for the P2VP38k sample arises from long wavelength concentration fluctuations when approaching a polymer-mediated network bridging type of phase transition as ϕ increases.[27] The theory with validated parameters further provided a real space physical picture of the nanometer-scale microstructure: at $\phi = 0.16$, the nearest-neighbor coordination number of tightly bridged NPs is ≈2, suggesting the onset of a percolated network at this loading. Interestingly, this theoretical result is in good agreement with the rheology data for the P2VP38k sample (Figure 1a). At $\phi = 0.27$, PRISM theory predicts the number of bridging nearest neighbors to be ≈4.[27] Such an increase is physically expected and qualitatively consistent with the large value of ΔE deduced from rheology data in Figure 1. It should also be emphasized that the theory predicts that the bridges are very tight (1−2 segments thick),[27] and hence we expect that polymer M_w will have a very minor effect on the number of tightly bridged NPs.

If a truly random NP dispersion was achieved, various structural parameters, including the average interparticle separation distance (ID), can be estimated based on the primary peak position q^* in $S(q)$ (see, Table S1). However, TEM images (Figure S3) show clear evidence of local clustering (as predicted by PRISM theory)[27] in all the PNC samples, which is expected due to polymer-mediated bridging of NPs, indicating a locally heterogeneous microstructure and a broad distribution of ID, which is consistent with a broad peak in $S(q)$ (Figure 2). Hence, though often reported in PNC studies, the structural parameters tabulated in Table S1 may not be physically relevant. In this article, we therefore aim to establish the correlations between the material properties and the collective NP dynamics/structures as a function of NP loading instead of the widely used "polymer chain confinement" defined as $ID/2R_g$[18,30] computed assuming random NP dispersion.

Collective NP Dynamics. The collective NP dynamics in the P2VP matrix are investigated with *in situ* XPCS to measure the local motions of "markers"[38] (*i.e.*, SiO_2 NPs which have a high X-ray contrast with the polymer) over a wide range of q space ($q = 0.05-0.4$ nm^{-1}) and time scales ($10^{-3} < t < 10^3$ s). We note that although these time scales can be viewed as "long" relative to those of the pure polymer melt at high temperatures, they do not need to be for the collective dynamics and self-diffusion of the 18−24 nm diameter NPs dissolved in the viscous polymer matrices that we study. For example, for a single NP of 20 nm diameter in a P2VP38k melt at 180 °C, the characteristic elementary Stokes−Einstein diffusion time scale is $\tau_{SE} \approx 2$ s (if one estimates the time per Fick's law as $(2R_N)^2/6D_{SE}$, where D_{SE} is the NP diffusion constant calculated from the Stokes−Einstein (SE) relationship (see below)). Moreover, since terminal flow of the PNCs at high NP loadings is not observed (unmeasurable low-frequency viscosity), long time/distance Fickian diffusion of the NPs seems impossible on the XPCS time scale. Hence, our XPCS measurements are probing the relatively "short" time and length scale collective motions of NPs as influenced by the viscous friction associated with the vast majority of the polymer matrix and the constraints imposed by the small fraction of polymer segments that constitute long-lived bridges. If this physical picture is correct (as we argue below), one would expect a relatively simple time decay (*e.g.*, roughly exponential) of the XPCS collective dynamic structure factor.

The XPCS intensity−intensity autocorrelation function g_2 is calculated from the intensity of pixel variations in the time series of the speckle patterns collected during the measurement. The experimentally determined $g_2(q,t)$ is fit to a Kohlrausch−William−Watts (KWW)-type exponential in the form of eq 2 with a relaxation time, τ, and stretching exponent, α. The Siegert factor (B), which depends on the experimental set up, and the baseline (c) are additional fit parameters.[39]

$$g_2(q, t) = B\left(\exp\left(-2\left(\frac{t}{\tau}\right)^{\alpha}\right)\right) + c \tag{2}$$

An example of dynamics resolved by XPCS in terms of $g_2(q,t)$ and the fit with eq 2 are shown in Figure 3a for the PNC with

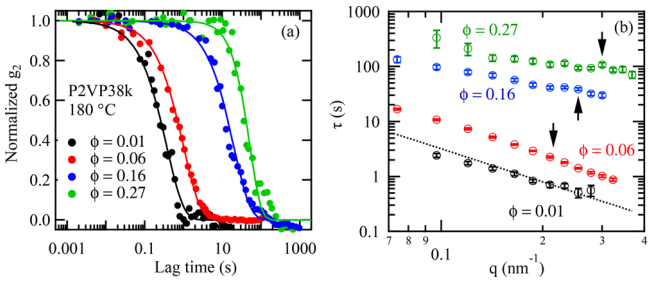

Figure 3. (a) Representative XPCS data for the P2VP38k samples at representative q = 0.23 nm^{-1} and 180 °C. The solid lines correspond to the best-fits of eq 2 to the data; $\alpha = 1$ for $\phi = 0.01$, 0.06, and 0.16, while $\alpha = 1.35$ for $\phi = 0.27$. (b) Relaxation time τ *vs* q for the P2VP38k series at 180 °C. The dotted line shows the time scale associated with SE limit of diffusivity. The arrows correspond to the q^* positions.

P2VP38k. Here, g_2 is normalized by B and the baseline for clarity ($(g_2 - c)/B$). Over the limited amplitude (vertical) scale probed in the measurement (shown on a linear scale in Figure 3a), the correlation functions decay on an observable time scale and can be reasonably well fit to eq 2 with $\alpha = 1 - 1.5$ (Figure S4). It is likely that $\alpha = 1$ can be justified for the $\phi = 0.01$, 0.06, and 0.16 samples regardless of q used in this study, while modestly compressed ($\alpha > 1$) relaxations ($\alpha \approx 1.3$ in Figure 3 and Figure S4) are seen for the P2VP9k and P2VP38k samples at $\phi = 0.27$. We note that $\alpha = 1$ corresponds to a simple exponential decay, which implies the forces on NPs are rapidly relaxing compared to the experimental time scale of NP motion observed, the so-called "Markov limit". This is a major simplification since the dynamics is characterized by a single average time scale, a feature that will be exploited in our theoretical analysis below. The B values in eq 2 were approximately 0.08 regardless of temperature, ϕ, and M_w and are comparable to those found for a static porous glass sample (CoralPor, SCHOTT), suggesting that the sample did not exhibit faster dynamic modes outside of our time window.

From Figure 3b, one sees that the τ values for the P2VP38k samples increase with ϕ (the same is true for the series of P2VP9k (Figure S5)), where at the highest NP loadings τ is

https://doi.org/10.1021/acsnano.1c01283
ACS Nano 2021, 15, 11501−11513

observed to increase by 2 orders of magnitude compared to that at $\phi = 0.01$. From a colloid or NP suspension perspective, a two-decade increase is relatively modest and is not representative of approaching a glass transition, consistent with the present XPCS temporal decay observed to be of a one-step form (no transient plateau or two-step decay). We note that a similar XPCS result was previously reported in SiO_2 NPs embedded in entangled poly(ethylene oxide) melts.[40]

Figure 3b also shows the q dependence of τ for the P2VP38k series at 180 °C. For the dilute P2VP38k sample at $\phi = 0.01$, one sees $\tau \sim q^{-\gamma}$ with $\gamma = 2$, which corresponds to a simple diffusive motion. However, the measured NP diffusion constant ($D_N = 1/(\tau q^2)$) is found to be smaller than those predicted by the SE relationship:

$$D_{SE} = k_B T/(6\pi R_N \eta_0) \quad (3)$$

where k_B is the Boltzmann constant, T is the absolute temperature, and η_0 is the zero-shear rate viscosity of the bulk P2VP matrix (Table S2). This observation is consistent with the data of Winey and co-workers[18] for a similar dilute SiO_2(R_N = 13 nm)/P2VP system using Rutherford backscattering spectrometry. To account for the modest deviation, they modified the SE relationship as follows:

$$D_N = k_B T/(6\pi R_E \eta) \quad (4)$$

assuming the effective NP radius (R_E) includes a BPL of thickness $R_E = R_N + 1.1R_g = R_N + 0.0305 \times M_w^{0.5}$ (nm) for SiO_2/P2VP PNC systems.[18] The zero shear rate viscosity, η, of a dilute loaded PNC is estimated by using the following relationship:[18]

$$\eta = \eta_0(1 + 2.5\phi_{eff} + 6.2\phi_{eff}^2) \quad (5)$$

where ϕ_{eff} is the effective NP volume fraction ($\phi_{eff} = \phi(R_E/R_N)^3$). As shown in Figure 3b, the q dependence of τ for the P2VP38k 1% sample is in good agreement with that predicted by the modified SE relationship (eq 5, indicated by the dotted line in Figure 3b), as previously validated.[18] Consequently, the collective dynamics detected by XPCS in the dilute NP limit tracks the self-diffusion of individual NPs (coated with the BPL) embedded in the viscous polymer matrix.

On the other hand, it is clear from Figure 3b that the collective NP dynamics in the PNCs qualitatively deviate from the simple diffusive behavior as NP loading increases. It is also notable that the relaxation time grows monotonically with decreasing wavevector except for the 6%, 16%, and 27% samples in the high wavevector "cage" regions around the peak of $S(q)$ at $q \approx q^*$ (Figure 2), where the relaxation time exhibits a shallow maximum (see, Figure S5 for the P2VP9k series and Figure 3b for the P2VP38k series). The latter nonmonotonic behavior is reminiscent of the so-called de Gennes narrowing effect,[41] where the collective relaxation time is proportional to $S(q)$ in the region near a cage peak $q \approx q^*$. Our systems do show a cage peak in $S(q)$, but it is very weak (Figure 2), consistent with the weak nonmonotonic variation of the relaxation time observed experimentally. As will be described later, both the shallow maxima in $S(q)$ and $\tau(q)$ at $q \approx q^*$ seen in the experiments for all NP volume fractions are captured very well by the NP size polydispersity-corrected PRISM and MCT theories. In addition, we find that τ becomes less dependent on q at the higher loadings for the high and intermediate wavevectors and shows an interesting *weakly nonmonotonic* variation of the slope in $\tau(q)$ in the low q regime, that is, $q < 0.2$ nm^{-1}, as shown quantitatively in Figure S6.

In order to test whether there is a "generic" (to leading order) q dependence of the relaxation times at fixed loading regardless of NP diameter, temperature, or polymer molecular weight, we plot all our relaxation time data in Figure 4

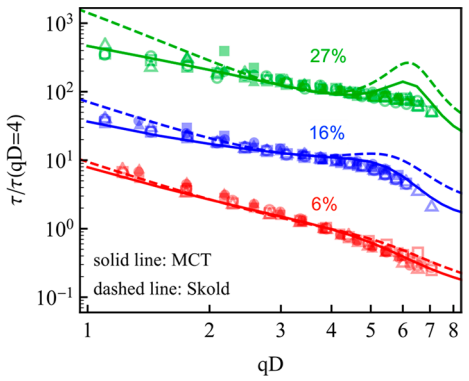

Figure 4. Collapsed qD dependence of collective relaxation times (τ). The τ values are normalized by the τ value at $qD = 4$. Vertical shifts (10 for $\phi = 0.16$ and 100 for $\phi = 0.27$, respectively) are used for clarity. Filled (P2VP38k) and open (P2VP9k) symbols represent the data set for different MWs at 160 °C (square), 170 °C (circle), and 180 °C (triangle). Solid and dashed lines are theoretical predictions based on MCT and Skold approximations, respectively.

adopting a reduced dimensionless wavevector (*i.e.*, qD) with τ normalized by its value at $qD = 4$ (arbitrary choice) for each loading. One sees that to a zeroth order, across all temperatures and M_w, there is a *rough* collapse to a master curve within the experimental uncertainties. As discussed theoretically below, this suggests the behavior of $\tau(q)$ is essentially polymer chain length *independent* if one normalizes out (to zeroth order) the elementary ensemble-averaged polymer time scale in the PNCs (which is T and M_w dependent).

Finally, we comment on the compressed exponential form for the highest loading PNCs. At present, there is no theoretical understanding of its origin nor even a qualitative consensus about its microscopic origin.[42] This feature is not special to PNCs, but is seen in a wide range of soft matter systems.[43] Understanding it is not a goal of our present work. Moreover, to test its relevance to the conclusions we have drawn, we have carried out the practical exercise of extracting $\tau(q)$ from when the measured time correlation function decays to a value of $1/e$ (Figure S7), *versus via* fitting to eq 2. We find that our results for the q dependence of $\tau(q)$ and the master curve in Figure 4, and its dependence on loading, polymer M_w and T, are *not* sensitive to the method of determining the 27% loading sample relaxation time. This strongly suggests that the underlying physics of the trends we have established for the collective relaxation time are not causally connected with the compressed exponential feature, which is a simplifying finding we exploit in the theoretical analysis below.

Theory Formulation. To the best of our knowledge, there exist no predictive microscopic theories for essentially any aspects of the collective NP dynamics in PNCs. The basic challenge is to understand the XPCS relaxation time as a function of the four experimental control variables, $\tau = \tau(q, \phi, T, M_w)$, including how inter-related the observed dependences

https://doi.org/10.1021/acsnano.1c01283
ACS Nano 2021, 15, 11501−11513

are. The results in Figure 4 suggest that this four-dimensional function may factorize, to leading order, into a product of a q- and ϕ-dependent function (reflecting polymer-mediated NP collective dynamics) that is *independent* of chain length to leading order, multiplied by a T- and M_w-dependent function that sets an elementary time scale associated with friction on NPs due to the dynamics of the polymer matrix. If the polymer subsystem dynamics was unperturbed by NPs from the segmental to chain scales, as suggested by recent ensemble-average dielectric measurements,[37] then this elementary time scale would be proportional to the SE time discussed above, τ_{SE}, computed using the pure polymer melt viscosity. Moreover, if the polymer dynamics was fast (effectively equilibrated) compared to the collective NP motions probed in the experiments (as suggested by a recent combined viscoelastic and dielectric experimental study),[37] then, at least in an average sense, polymers influence collective NP dynamics in two ways: (i) modify their equilibrium microstructure (*e.g.*, bridges, adsorbed layers) as embedded in $S(q)$, and (ii) set the elementary time scale we define as τ_0 associated *via* the friction they exert on a NP. Naive adoption of this physical picture would suggest $\tau_0 \approx \tau_{SE}$, and that the XPCS data can be analyzed based on an effective one-component NP fluid in a viscous medium. The rich dependence of the XPCS relaxation time on loading and wavevector would then reflect how the NP spatial correlations modify effective forces between NPs and the background viscous friction due to the polymer matrix.

Our present theoretical attempt to address this problem adopts the above physical scenario to study the wavevector and NP loading dependence of the XPCS relaxation time. In essence, we ask how much of the complex NP collective dynamics measured by XPCS can be traced back to the polymer-mediated collective NP equilibrium structure? The presented analysis effectively assumes that a time-scale separation between the NP and polymer subsystems exists in a mean ensemble-averaged sense for the purpose of predicting NP collective dynamics on the (relatively short) time and length scales probed by XPCS. Given the loadings studied are not close to a pure NP suspension or viscous liquid glass transition, the analogous problem is a modestly concentrated fluid or suspension where NPs experience space−time correlated forces, the consequences of which are related to the polymer-mediated nonrandom microstructure that evolves with q and ϕ.

The microscopic MCT is a natural tool to address this dynamical problem.[44,45] Since one is far from a glass transition, and we believe XPCS is probing the relatively short time- and length-scale collective dynamics, it is the simpler, so-called "non-self consistent", version[46] that is appropriate. Physically, this corresponds to the forces that impede NP motion relaxing on faster time scales than the collective NP relaxation process ("Markov regime"). The dynamical q-dependent generalized longitudinal stress memory function involves a diffusive very short time/distance friction component, and a longer length- and time-scale component associated with effective inter-NP forces determined from the microstructure, $S(q)$, which relaxes more slowly *via* a cage diffusion mechanism as well verified for moderately dense hard sphere colloidal suspensions[47] (see SI for the details).

To implement the dynamical theory requires the NP collective structure factor, $S(q)$, as input. It would be ideal to use the "exact" experimentally measured structure factor as input. However, this is not feasible, due largely to the limited range of wavevectors in $S(q)$ known from the X-ray scattering measurements. Hence, we adopt the PRISM integral equation theory of PNCs to compute $S(q)$. A well-studied minimalist model is employed defined by NPs as monodisperse in diameter hard spheres, polymers as semiflexible bead chains of degree of polymerization N, and one effective interfacial attraction parameter to account for segment-NP cohesion. The parameters of this model are taken from our prior study of the same silica-P2VP samples,[27] where they were determined by optimizing agreement between theory and experiment for the features of $S(q)$ of central importance in that work. We set N = 100, a sensible value for the P2VP9k series. However, many prior PRISM theory and simulation studies of PNCs have found that the NP $S(q)$ is largely insensitive to N in dense melts with small static density correlation lengths. Hence, we keep N fixed in our present work, a simplification also consistent with our experimental finding that the normalized $\tau(q)$ in Figure 4 is not M_w sensitive. Of course, N may explicitly matter for some dynamical phenomena due to the potential importance of entanglements, glassy bridges, or other effects not taken into account in our initial dynamical theory based on a presumed separation of time scale between (fast) polymers and (slow) NPs.

The MCT equation of motion for the collective dynamic structure factor, $S(q, t)$, under the conditions described above can be solved in the relevant Markov regime (see SI) to obtain $S(q, t)/S(q) = e^{-t/\tau(q)}$, where the collective relaxation time is

$$\tau(q) = \frac{S(q)}{q^2 D_s}\left(1 + \frac{\rho}{16\pi^2}\int_0^\infty d\mathbf{k}\frac{|V_{\mathbf{k},\mathbf{q}-\mathbf{k}}|^2}{k^2/S(k) + (\mathbf{q}-\mathbf{k})^2/S(|\mathbf{q}-\mathbf{k}|)}\right) \quad (6)$$

The second contribution in eq 6 reflects the effect of microstructural correlations on NP collective dynamics, with a so-called "force vertex" quantified by effective inter-NP forces and pair structure as $V_{\mathbf{k},\mathbf{q}-\mathbf{k}} = (\hat{\mathbf{q}}\cdot\mathbf{k})C_{eff}(k) + \hat{\mathbf{q}}\cdot(\mathbf{q}-\mathbf{k})C_{eff}(|\mathbf{q}-\mathbf{k}|)$. Here, the effective NP−NP direct correlation function $C_{eff}(q) = 1/\rho - 1/(\rho S(q))$, where $S(q)$ is computed using PRISM theory of PNCs for size monodisperse NP spheres,[48] ρ is the particle number density, and $\mathbf{q}$ and $\mathbf{k}$ are wavevectors, $q = |\mathbf{q}|$ and $\hat{\mathbf{q}} = \mathbf{q}/|\mathbf{q}|$. The leading short-time diffusive-like contribution in eq 6 is computed in the spirit of an effective collision model[47] as $D_s = D_0/g(\phi_{eff})$; here the elementary NP diffusion coefficient D_0 is related to the polymer friction on a single NP, and $g(\phi_{eff})$ is the contact value of the corresponding effective hard-sphere system $g(r)$ at an effective volume fraction $\phi_{eff} = 2.2\phi$ (see SI). This expression for the short time diffusivity is well-known to be very accurate in hard sphere colloidal suspensions.[47]

We acknowledge that in PNCs the elementary diffusivity D_0 may involve complex polymer physics as has been probed, for example, *via* polymer center-of-mass diffusion measurements in PNCs.[23] As discussed above, as a zeroth-order approximation, we assume D_0 is simply related to the neat polymer viscosity *via* the SE relation, which sets the elementary time scale $\tau_0 \equiv (2R_N)^2/D_0$. The MCT-based approach adopted does accurately capture[49] the growth of the q-dependent structural relaxation time and shear viscosity, and decrease of the self-diffusion constant, in hard sphere colloidal suspensions over a wide range of (preglassy regime) packing fractions where these properties change by a factor of 30−100. The latter nonperturbative, but relatively modest, factor is close to the

https://doi.org/10.1021/acsnano.1c01283
ACS Nano 2021, 15, 11501−11513

magnitude of changes we observe as NP loading increases in our XPCS experiments (Figure 3b).

To gain more insight about NP collective dynamical effects, we also consider a simpler model for the XPCS relaxation time called the Skold approximation.[50] It relates the collective dynamics to *single* particle motions modified by the static microstructural correlations yielding a relaxation time of a *generalized diffusive* form:

$$\tau(q) = \frac{S(q)}{q^2 D_L} \tag{7}$$

The corresponding q-independent self-diffusion constant can be obtained from the same level of dynamical theory embedded in eq 6:[51]

$$D_L = D_s\left(1 + \frac{\rho}{6\pi^2}\int_0^\infty dq q^2 \frac{C_{eff}^2(q)S(q)}{1 + 1/S(q)}\right)^{-1} \tag{8}$$

where D_L is the "longer time" diffusion constant that includes *both* the short time binary collision physics and contributions from local many particle caging or microstructure due to multiple space-time correlated dynamical events. Eq 7 is typically accurate in a limited wavevector range straddling the wavevector (q^*) of the cage peak in $S(q)$, and for nonglassy thermodynamic states, or the short time "pre-transient localization" dynamics of glassy systems.[52]

The $S(q)$ required to calculate $\tau(q)$ is computed using the PRISM theory with a single effective interfacial attraction energy model as previously parametrized for the P2VP38k system at 180 °C.[27] In thermal energy units, the segment−NP contact attraction energy ($\beta\epsilon_{pn}$) is $\beta\epsilon_{pn}$ = 5.2. As discussed above, given the minor effect of temperature and M_w on $S(q)$ from our SAXS measurements, we adopt the same $S(q)$ input for dynamical calculations relevant to the P2VP9k and P2VP38k systems at 160, 170, and 180 °C.

Comparison of Experiment and Theory. We first compare the theoretical *predictions* for the q dependence of $\tau(q)$ with our XPCS measurements. These comparisons are *not* fits; only vertical shifting to align theory and experiment is done. As shown in Figure 4, the MCT-based results (with a fixed value of N) capture quite well the q dependence and its variation with NP loading. The only obvious discrepancy is the peak at $q \approx q^*$ (the cage peak region of $S(q)$) for the 27% loading sample is too strong. In general, a leveling off of $\tau(q)$ in the low q-region (*i.e.*, $qD < 3$) is also observed as ϕ increases. A closer examination of the experimental data shows that the change of slope in $\tau(q)$ is slightly *nonmonotonic* with the 16% being the weakest (Figure S6), and this subtle feature is captured by the theory. In comparison, the Skold approximation that ignores explicit collective *dynamical* effects predicts the q dependence at low q becomes monotonically stronger with loading, which clearly deviates from the experiments. In addition, at high NP loadings, the Skold model overpredicts $\tau(q)$ at $q \approx q^*$, while the MCT performs quantitively better. The trend that both the dynamical theories predict well-defined peak-like features around $q \approx q^*$ for the highest NP loading is very likely due to the overprediction of the cage peak of $S(q)$ since our model is monodisperse in NP diameter, *versus* weakly polydisperse in experiment, as discussed in our prior work.[27] Evidence for this is the fact that the experimental cage peak intensity in Figure 2 is much weaker than predicted by PRISM theory for the monodisperse NP model (see Figure S8).

The physics underlying the interesting nonmonotonic evolution of the q dependence of $\tau(q)$ with loading in the small and intermediate wavevector regimes can be revealed by dissecting the contributions from the short-time diffusion and collective dynamics to the total $\tau(q)$ in eq 6. Figure 5 shows

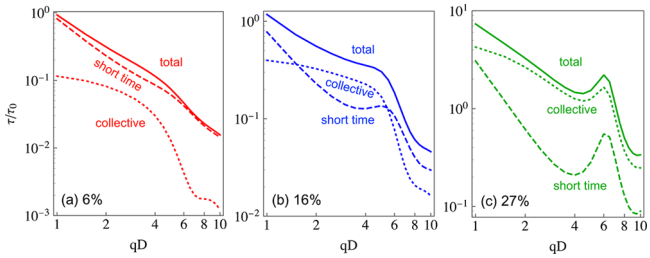

Figure 5. Short-time and collective contributions (first and second terms on the right-hand side of eq 6, respectively) to the total q-dependent collective relaxation time normalized by the elementary time scale τ_0 based on MCT for different NP loadings.

the results. It is evident that the relative importance of the two contributions changes from the short-time diffusive process dominating at ϕ = 0.06 to the slower nondiffusive collective contribution dominating at ϕ = 0.27, while they are comparable at ϕ = 0.16, a physically intuitive evolution with NP loading. Given the different q dependences of these two dynamical contributions, which also evolve moderately with loading, we conclude it is the competition between local short-time diffusion and the many NP collective dynamics that leads to the nonmonotonic change of the $\tau(q)$ slope. Since the Skold approximation ignores the *explicitly dynamical* component of collective effects, this explains its failure to capture this feature.

We now consider the NP loading dependence of the collective NP dynamics. Figure 6 shows the theoretical and

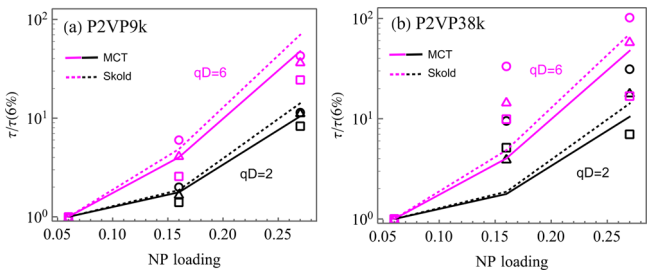

Figure 6. NP loading dependence of the relaxation times τ normalized by their 6% values at the low q (qD = 2, black) and high q (qD = 6, magenta) for the P2VP9k and P2VP38k series. Squares, triangles, and circles correspond to the data at 160 °C, 170 °C, and 180 °C, respectively. Theoretical predictions based on the MCT (solid lines) and the Skold approximation (dotted lines) are shown.

experimental $\tau(q)$ results at fixed low and high wavevectors, qD = 2 and 6, as a function of NP loading normalized by their 6% values at different temperatures. The theory qualitatively captures the overall growth of the relaxation time by a factor of 10−100. Roughly 90% (50%) and 10% (50%) of this growth emerges from the short time friction (contact value) and many particle microstructural part in eq 6, respectively, at qD = 2

https://doi.org/10.1021/acsnano.1c01283
ACS Nano 2021, 15, 11501−11513

(qD = 6). The weakening of the wavevector dependence observed in our experiments is clearly a collective effect.

Quantitatively, the MCT predictions in Figure 6 are in very good agreement with the unentangled (and smaller R_g) P2VP9k data, which also appears to be insensitive to temperature. For the weakly entangled (and larger R_g) P2VP38k systems, the theory underpredicts the increase of $\tau(q)$ with ϕ around 16% loading, and a larger temperature effect is observed. These discrepancies might be due to our assumption of a loading independent bare friction constant (*via* τ_0) set by the neat polymer, which apparently is reasonable for P2VP9k but not for the P2VP38k systems, possibly reflecting complicated effects of temperature and M_w on D_0 or τ_0.

Interestingly, the Skold model predictions in Figure 6 based on eq 8 are very similar to those of the full MCT. We thus conclude that "collective q dependent" effects embedded in eq 6 are much less important for how the XPCS relaxation time grows with loading, that is, the friction associated with single particle diffusion in the PNC captures well the slowing down of collective relaxation with loading at both small (qD = 6) and intermediate (qD = 2) length scales.

A question of materials chemistry and physics interest is the influence of the precise magnitude of the polymer segment-NP interfacial adsorption energy, $\beta\epsilon_{pn}$, on our dynamical predictions. Figure S10 shows the effects of $\beta\epsilon_{pn}$ are relatively minor, but not negligible.

One can also ask how sensitive our theoretical results are to the background matrix being a polymer melt? In the dynamically effective one-component model adopted, polymer physics enters *via* the NP microstructure, $S(q)$. To address the raised question, we crudely treat PNCs as an effectively one-component hard sphere colloidal suspension following standard ideas,[44] as discussed in SI. The corresponding dynamical predictions are shown in Figure S11, and one sees two major qualitative failures compared to the experiments. First, the q dependence of $\tau(q)$ at low q become flatter and evolves monotonically with NP loading, likely as a result of negligible collective effects at ϕ = 0.27 for hard sphere fluids since there is no polymer-mediated bridging. Second, there is an inversion of loading dependence at $qD \approx 4$, below which faster dynamics is predicted as loading increases, in qualitative contrast with the experimental data.

The final part of our theoretical analysis concerns the influence of weak NP size polydispersity present in the experiment but ignored in the above theoretical analysis. We believe this will affect mainly the sharpest feature of $S(q)$ and $\tau(q)$, the peaks at $q \approx q^*$ in Figures 2 and 4, respectively, which are overpredicted in intensity by the monodisperse NP theory. How continuous NP size polydispersity should be accounted for in the PRISM and MCT approaches for PNCs is an open theoretical problem. However, we have formulated a simple approximation for this problem in section II E of the SI and repeated the calculations in Figures 4 and 6 using experimentally relevant degrees of polydispersity. As shown in the SI, both the small intensity of the cage peak in $S(q)$ seen in the experiments for all NP volume fractions, and the much weaker maximum in $\tau(q)$ at $q \approx q^*$ are *simultaneously* captured very well by the polydispersity-corrected theories (Figures S14 and S15). Very importantly, the results in the SI show that polydispersity does *not* change any of our other basic predictions obtained using the monodisperse model, including the subtle nonmonotonic evolution with NP loading of the apparent slope of $\tau(q)$ in the lower wavevector regime discussed above.

Finally, as described below, we have experimentally found interesting (and coupled) behaviors for how the XPCS relaxation time evolves with temperature and polymer M_w. The former involves qualitative deviations from naive expectations, while the latter is more quantitative in nature. In either case, these aspects have not yet been addressed theoretically. We believe they require formulating a predictive polymer physics theory for the motion of polymers in the confined and adsorbing spaces between NPs, and perhaps a more explicit treatment of the small fraction of polymer segments in the dynamically slower tight bridges, which are open theoretical challenges beyond the scope of this work.

Temperature Dependence. We have measured the effect of temperature on $\tau(q)$ over a narrow range between 160 and 180 °C for the P2VP9k and P2VP38k series. Figure 7a shows the results with $\tau(q)$ normalized by its value at 180 °C at qD = 2 and qD = 6. Figure 7b summarizes the relaxation times at 160 °C normalized by those at 180 °C for the P2VP9k and

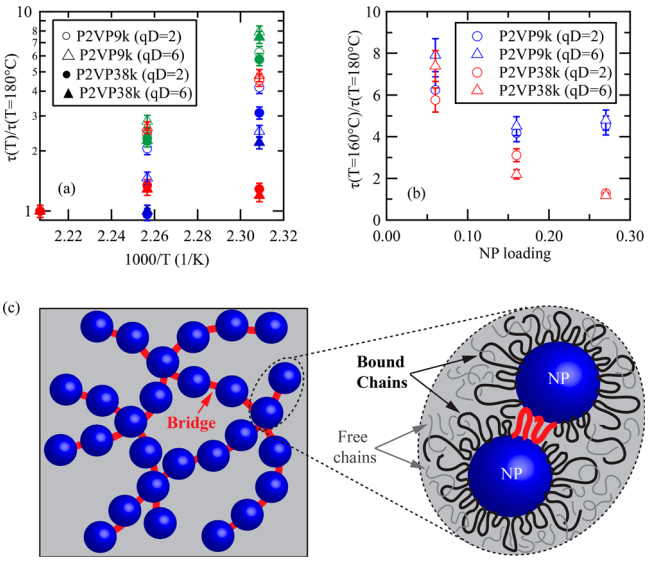

Figure 7. (a) Temperature dependence of the normalized relaxation times at qD = 2 and qD = 6 for the P2VP9k and P2VP 38k series. The colors correspond to data collected at ϕ = 0.06 (green), ϕ = 0.16 (blue), and ϕ = 0.27 (red). (b) Relaxation times at 160 °C normalized by those at 180 °C at qD = 2 (represented by circles) and qD = 6 (represented by triangles) for the P2VP9k (blue symbols) and P2VP 38k (red symbols) series. (c) Cartoon of NP network structures at high loading $\phi > \phi_c$. NPs are represented by blue circles connected by tight polymer bridges (represented by red lines). The model of a "string-like" network is motivated by the TEM image at ϕ = 0.06 (Figure S3b), where the NPs line up as locally favored clusters. The right figure shows a cartoon of plausible chain structures near the polymer/NP interface. A few tails and/or loops composed of the BPL adsorb on the surfaces of neighboring NPs concurrently, resulting in the formation of "doubly adsorbed" polymer segments (*i.e.*, polymer bridges indicated in red). For entangled chains, the tails and (large) loops of the BPL can entangle or interdigitate with free chains in a matrix. We caution that in a dense melt (*versus* relatively dilute solution), polymer bridges do not consist of a single chain connecting two NPs. Rather, they represent a small piece of the polymer melt (multiple chains) that forms a thin cohesive structure that adsorbs on two NPs and spans the gap region of closest approach between them.

https://doi.org/10.1021/acsnano.1c01283
ACS Nano 2021, 15, 11501−11513

P2VP38k series as a function of ϕ. From the figures, we find that the role of qD in the temperature dependence is minimal (*i.e.*, the normalized relaxation times are nearly identical regardless of a choice of qD), suggesting that the unusual temperature dependence is somehow related to the polymer subsystem and hence τ_0 in our theoretical model. In addition, for the P2VP9k series, the temperature dependence of the reduced τ seems to be insensitive to ϕ (Figure 7b). This trend stands in contrast to the significant dependence of the PNC rheological shift factors on loading in Figure 1, though it is qualitatively consistent with dielectric measurements of the polymer subsystem relaxation on segmental and chain scales.[37] Quantitatively, we note that the viscosity of the neat P2VP9k and P2VP38k melts decreases by factors of about 4.4 and 9.2, respectively, when the temperature increases from 160 to 180 °C (Table S2). It should be noted that the thickness of a BPL and the corresponding *ID* between neighboring NPs, which affect the properties of the PNC, is weakly temperature dependent. Hence the effective viscosity of the PNC may deviate from the pure polymer melt, although these effects should be very small over the very narrow range of temperature used in this study. Since both the ensemble-averaged segmental relaxation[17,25,37] and the chain relaxation[37] of a matrix polymer in high loading PNCs remain essentially unchanged relative to those of the neat polymer, we expect that the temperature dependence of the collective NP dynamics tracks the viscosity change of a matrix polymer. As a speculative comment, the unexpectedly weak temperature dependence for NP collective relaxation reflects at ϕ = 0.16 and ϕ = 0.27 an overdamped collective "vibration-like" character for their motion enforced due to long-lived (but very low volume fraction) polymer bridges, as schematically shown in Figure 7c.

For the P2VP38k series, we observe an even more unusual behavior: The temperature dependence of the reduced τ becomes significantly *weaker* with increasing ϕ. As we commented on above in the context of the role of compressed exponential relaxation, it should be noted that this unusual temperature dependence does *not* reflect the method of τ extraction from the observed g_2 functions (Figure S6). Interestingly, Winey and co-workers reported a similar unusual temperature dependence of the polymer center-of-mass tracer diffusion coefficient (D_t) in athermal PNCs composed of SiO_2 NPs (D = 28.5 nm) and entangled polystyrene (M_w = 650 kg/mol).[53] The D_t value (measured by using elastic recoil detection) relative to the neat melt was reduced at higher temperatures: at $\approx T_g$ + 80 °C, the reduction in D_t at ϕ = 0.3 relative to the bulk melt was a factor of 3, while at T_g + 60 °C, it was about a factor of 2. They also argued that the reptation model,[54] the modified reptation model considering "particle entanglements" effects imposed by NPs,[25] or T_g changes in PNCs[53] cannot account for the unusual temperature dependence of polymer center-of-mass diffusion. Since their system is different from ours (*i.e.*, a sample geometry (thin films *versus* bulk films), polymer chain length, NP size, and NP−polymer interaction), their NP microstructures, including the question of whether they have a percolated network, may be different from our systems. Nevertheless, their results are noteworthy and may be relevant to the unusual T dependence of our XPCS measurements. For example, the difference of the collective NP dynamics temperature dependence of P2VP9k *versus* P2VP38k might be related to the reduction of available chain conformations in the presence of NPs which reduces the chain diffusivity.[55] Further XPCS experiments are required to definitively understand whether entanglement effects, geometry (R_g/R_N), confinement (ID), or some other microscopic mechanism underlies the unexpected T dependence of the XPCS relaxation times.[56−58] Before leaving this issue, we offer a specific idea that could be relevant.

A unique feature of PNCs relative to pure polymer melts is there are potentially entanglements between the bound (adsorbed) chains and free (matrix) polymer chains at the polymer−NP interface. As sketched in Figure 7c, the vast majority of the BPL is *not* in bridges, but rather at the level of individual chains in the tails and large loops which can entangle or interdigitate with free matrix chains.[59] This could lead to an additional interfacial friction which slows down NP motion in PNCs. Neutron scattering/spectroscopy experiments using selective isotope labeling[20] on carbon black or SiO_2 filled elastomers were recently performed to directly probe the interfacial dynamics of the BPL at the segmental and chain levels in a chemically identical polymer matrix. The results support the idea of interfacial entanglements/interdigitation at the bound polymer-free polymer interface, as will be discussed in a forthcoming paper.

Phenomenologically, the temperature dependence of the collective NP dynamics shown in Figure 7a is suggestive of Arrhenius-type activated process with an activation energy (E_a) that follows as

$$\ln[\tau(T)/\tau(180\,^{\circ}\mathrm{C})] = \frac{E_a}{RT} + A \tag{9}$$

where R is the gas constant (8.314 J/K mol) and A is a numerical constant. As tabulated in Table S1, we find that the E_a values extracted from our XPCS data *decrease* with increasing ϕ for the P2VP38k series. A similar ϕ dependence of E_a is evidenced for the P2VP9k. Nevertheless, this is the *opposite* trend of the aforementioned rheology/mechanical response (Figure 1c). This suggests that whatever the trajectory-level nature of the collective NP motions is, it does not involve the irreversible dynamic reorganization of the (perhaps "glassy") polymer bridges that have been argued to be long-lived and critical to PNC rheology.[30] This opposite T dependence also suggests the collective NP dynamics probed by XPCS may not be directly crucial for bulk PNC viscoelasticity, a deduction seemingly consistent with the key long-lived stresses arising from polymer bridges that mechanically connect NPs into a percolated network.

CONCLUSIONS

In conclusion, we have presented an integrated experimental XPCS and theoretical study of the rich collective dynamics of spherical silica NPs connected with polymer bridges in unentangled and weakly entangled P2VP matrices over a narrow range of temperatures (at $T \gg T_g$) and a wide range of NP loadings and length scales (wavevectors, q). The results demonstrate a generic q dependence of the NP collective relaxation times for the two PNCs series. Quantitative analyses shed light on the complex behavior as a function of probing length scale (wavevector), filler loading below and above the mechanical percolation threshold, temperature, and matrix polymer molecular weight. MCT calculations which include effective binary collisions and larger length scale and slower collective dynamics with the correct PNC microstructure input capture well all the XPCS results for the unentangled PNCs, while deviations are found for the temperature and loading

https://doi.org/10.1021/acsnano.1c01283
ACS Nano 2021, 15, 11501−11513

dependences in the entangled PNCs. A striking feature of the collective NP dynamics is its temperature dependence which is unexpectedly weakened at higher temperatures and higher NP loadings and qualitatively distinct from the temperature dependence of the rheology shift factors. This observation generically suggests some level of decoupling of collective NP motion from the dynamical processes that underlie mechanical stress relaxation in the PNC. Certainly, as NP loading grows, the number of polymer bridges per NP increases, leading to more constraints on NP motion as quantified in MCT by a change in microstructure. Though the microscopic mechanism of the discovered unusual temperature dependence is unresolved, it may involve interfacial entanglements, geometric confinement, or another mechanism related to how NPs modify polymer motion and the friction they exert on collective NP dynamics.

Finally, from a broader perspective, it is well-known from PNC rheology experiments that polymer bridges soften and can break (yielding) under modest applied strain,[11,12,29,37] a likely key component of the Payne effect and the Mullins effect.[60] It is also expected that polymer bridges rebuild when the distance and/or local stress between NPs is sufficiently small, responsible for the recovery properties of filler elastomers.[61] In operando XPCS experiments on the model PNCs subject to *in situ* oscillatory shear strain[62] would provide a further opportunity to establish connections between microscopic properties and macroscopic mechanical response associated with the complex coupled dynamics of polymer bridges and connected NPs.

METHODS

Materials. We use two collections of well-dispersed SiO_2 NPs synthesized by the Stöber method[63] and stabilized in ethanol with an average radius of R_N = 9.1 or 11.8 nm determined by SAXS experiments. Poly(2-vinylpyridine) (P2VP) with molecular weight M_w = 9 and 38 kg/mol and polydispersity of 1.1 was purchased from Specialty Polymers Inc. A series of PNCs with increasing volume fraction of NPs (ϕ = 0.01, 0.06, 0.16, and 0.27) were prepared by dropcasting and subsequent solvent evaporation. The details of the sample preparation have been described elsewhere.[27] NPs with R_N = 9.1 nm were used with the P2VP38k sample, while R_N = 11.8 nm was used with the P2VP9k sample. Samples were molded into circular disks and thermally annealed at 180 °C for 12 h.

X-ray Photon Correlation Spectroscopy Experiments. Temperature-dependent X-ray photon correlation spectroscopy (XPCS) measurements were conducted at Beamline 11-ID (Coherent Hard X-ray Scattering) of the National Synchrotron Light Source-II (Brookhaven National Laboratory) at three temperatures of 160, 170, and 180 °C. A partially coherent X-ray beam with energy of 9.65 keV (wavelength of λ = 0.128 nm) and unattenuated flux of 3×10^{11} photons/s was used. The beam size was approximately 40 μm × 40 μm (full width half-maximum). X-ray scattering patterns were collected on an Eiger X 4 M (Dectris) photon counting area detector with a 75 μm × 75 μm pixel size at a sample-to-detector distance of 10.8 or 16 m. After the sample was thermally equilibrated, measurements were performed at several sample locations, and the beam was attenuated for each data set to eliminate sample degradation and ensure dose independent dynamics. We confirmed that the characteristic times of the NP dynamics for all the samples remained the same on the time scale of the XPCS measurements. In XPCS, dynamics are resolved through an intensity−intensity auto correlation function g_2 (eq 10), which is derived from the time series of speckle patterns collected on the two-dimensional area detector during the XPCS measurements:

$$g_2(q, t) = \frac{\langle I(q, t')I(q, t' + t)\rangle}{\langle I(q)\rangle^2} \quad (10)$$

where $I(q,t')$ is the intensity at time t', and t is the delay time. The average $\langle ...\rangle$ is performed over all detector pixels corresponding to the same magnitude of the wavevector as well as over time.

SAXS Experiments. Small-angle X-ray scattering (SAXS) measurements were also conducted at Beamline 11-BM (Complex Material Scattering) of National Synchrotron Light Source-II (NSLS-II, Brookhaven National Laboratory) to further extend the high q region. The samples were placed on a thermal heating stage in transmission orientation and measured at 160 °C, 170 °C, and 180 °C with equilibration time of 15 min at each temperature before the measurements. The SAXS data were collected on a Pilatus 2 M detector (Dectris, a pixel size = 172 μm × 172 μm) at a sample to detector distance of 5 m, using an X-ray beam with the energy of 13.5 keV (the corresponding wavelength λ = 0.092 nm) and exposure time of 15 s. All scattering intensities $I(q)$ were corrected for sample transmission and background scattering.

TEM Experiments. Sample preparation for transmission electron microscopy (TEM) was done by using room-temperature ultramicrotomy (Leica UCT) and freshly prepared glass knives. Composite films were microtomed at a thickness of 50 nm and placed on copper grids with a 2−3 nm carbon support film. Imaging was performed using a JEOL JEM-2200FS Energy Filtered TEM at an accelerating voltage of 200 kV. All imaging was done utilizing zero-loss filtering with a slit width of 10 eV for providing enhanced contrast while staying close to focus (−200 nm under focus max).

Dynamic Mechanical Analysis. Rheological characterization was performed on a TA HR-2 and HR-3 Discovery rheometers using an 8 mm parallel plate geometry. Melt-pressed samples were loaded at 130 °C with a gap height of 0.7 mm and heated to 170 °C. Small amplitude oscillatory shear frequency sweeps were performed across a frequency range of ω = 0.1−100 rad/s at a strain amplitude of γ = 0.1%. The applied strain amplitude was found to be within the linear viscoelastic regime according to strain ramps from γ = 0.001−100% at 120 °C and ω = 10 rad/s. Frequency sweeps were performed from 120 to 176 °C. Time−temperature superposition principle was applied when appropriate.

ASSOCIATED CONTENT

Supporting Information

The Supporting Information is available free of charge at https://pubs.acs.org/doi/10.1021/acsnano.1c01283.

Additional details of the rheology data, the static SAXS data, TEM results of the PNCs, XPCS data analysis, structural parameters determined from the SAXS data, and theoretical background and additional results including the effects of NP polydispersity on the collective structure and dynamics (PDF)

AUTHOR INFORMATION

Corresponding Authors

Alexei P. Sokolov − *Chemical Sciences Division, Oak Ridge National Laboratory, Oak Ridge, Tennessee 37831, United States; Department of Chemistry, University of Tennessee Knoxville, Knoxville, Tennessee 37996, United States;* orcid.org/0000-0002-8187-9445; Email: sokolov@utk.edu

Kenneth S. Schweizer − *Department of Materials Science and Engineering, Materials Research Laboratory, and Department of Chemistry, University of Illinois, Urbana, Illinois 61801, United States*; Email: kschweiz@illinois.edu

Tadanori Koga − *Department of Materials Science and Chemical Engineering, Stony Brook University, Stony Brook, New York 11794-2275, United States; Department of*

Chemistry, Stony Brook University, Stony Brook, New York 11794-3400, United States; orcid.org/0000-0003-1316-6133; Email: tadanori.koga@stonybrook.edu

Authors

Benjamin M. Yavitt − *Department of Materials Science and Chemical Engineering, Stony Brook University, Stony Brook, New York 11794-2275, United States;* orcid.org/0000-0001-9308-7472

Daniel Salatto − *Department of Materials Science and Chemical Engineering, Stony Brook University, Stony Brook, New York 11794-2275, United States*

Yuxing Zhou − *Department of Materials Science and Engineering and Materials Research Laboratory, University of Illinois, Urbana, Illinois 61801, United States*

Zhixing Huang − *Department of Materials Science and Chemical Engineering, Stony Brook University, Stony Brook, New York 11794-2275, United States*

Maya Endoh − *Department of Materials Science and Chemical Engineering, Stony Brook University, Stony Brook, New York 11794-2275, United States;* orcid.org/0000-0001-6473-5047

Lutz Wiegart − *National Synchrotron Light Source II, Brookhaven National Laboratory, Upton, New York 11793, United States;* orcid.org/0000-0003-4417-8479

Vera Bocharova − *Chemical Sciences Division, Oak Ridge National Laboratory, Oak Ridge, Tennessee 37831, United States; Department of Chemistry, University of Tennessee Knoxville, Knoxville, Tennessee 37996, United States;* orcid.org/0000-0003-4270-3866

Alexander E. Ribbe − *Department of Polymer Science and Engineering, University of Massachusetts Amherst, Amherst, Massachusetts 01003, United States;* orcid.org/0000-0002-9924-3429

Complete contact information is available at: https://pubs.acs.org/10.1021/acsnano.1c01283

Notes

The authors declare no competing financial interest.

ACKNOWLEDGMENTS

The Donors of the American Chemical Society Petroleum Research Fund is acknowledged for support of this research (T.K.). T.K. also acknowledges partial financial support from Henkel Corporation and Brookhaven National Laboratory and National Science Foundation (NSF DGE 1922639). Y.Z., V.B., A.P.S., and K.S.S. acknowledge support for samples preparation, data analysis, and theory development by the U.S. Department of Energy, Office of Science, Basic Energy Sciences, Materials Sciences and Engineering Division. This work used resources of the Center for Functional Nanomaterials and the National Synchrotron Light Source II (Beamlines 11-ID and 11-BM), which are U.S. DOE Office of Science Facilities, at Brookhaven National Laboratory under contract no. DE- SC0012704. The authors thank Ruipeng Li, Masafumi Fukuto, Andrei Fluerasu, and Yugang Zhang for their help performing the SAXS and XPCS experiments and Dmytro Nykypanchuk and Shiwang Cheng for their help conducting the rheology experiments and analyzing the data.

REFERENCES

(1) Crosby, A. J.; Lee, J. Y. Polymer Nanocomposites: The "Nano" Effect on Mechanical Properties. *Polym. Rev.* **2007**, *47*, 217−229.

(2) Kumar, S. K.; Benicewicz, B. C.; Vaia, R. A.; Winey, K. I. 50th Anniversary Perspective: Are Polymer Nanocomposites Practical for Applications? *Macromolecules* **2017**, *50*, 714−731.

(3) Bailey, E. J.; Winey, K. I. Dynamics of Polymer Segments, Polymer Chains, and Nanoparticles in Polymer Nanocomposite Melts: A Review. *Prog. Polym. Sci.* **2020**, *105*, 101242.

(4) Kao, J.; Thorkelsson, K.; Bai, P.; Rancatore, B. J.; Xu, T. Toward Functional Nanocomposites: Taking the Best of Nanoparticles, Polymers, and Small Molecules. *Chem. Soc. Rev.* **2013**, *42*, 2654−2678.

(5) Yi, C.; Yang, Y.; Liu, B.; He, J.; Nie, Z. Polymer-Guided Assembly of Inorganic Nanoparticles. *Chem. Soc. Rev.* **2020**, *49*, 465−508.

(6) Akcora, P.; Kumar, S. K.; Moll, J.; Lewis, S.; Schadler, L. S.; Li, Y.; Benicewicz, B. C.; Sandy, A.; Narayanan, S.; Ilavsky, J.; Thiyagarajan, P.; Colby, R. H.; Douglas, J. F. Gel-Like" Mechanical Reinforcement in Polymer Nanocomposite Melts. *Macromolecules* **2010**, *43*, 1003−1010.

(7) Moll, J. F.; Akcora, P.; Rungta, A.; Gong, S.; Colby, R. H.; Benicewicz, B. C.; Kumar, S. K. Mechanical Reinforcement in Polymer Melts Filled with Polymer Grafted Nanoparticles. *Macromolecules* **2011**, *44*, 7473−7477.

(8) Genix, A.-C.; Bocharova, V.; Kisliuk, A.; Carroll, B.; Zhao, S.; Oberdisse, J.; Sokolov, A. P. Enhancing the Mechanical Properties of Glassy Nanocomposites by Tuning Polymer Molecular Weight. *ACS Appl. Mater. Interfaces* **2018**, *10*, 33601−33610.

(9) Jancar, J.; Douglas, J. F.; Starr, F. W.; Kumar, S. K.; Cassagnau, P.; Lesser, A. J.; Sternstein, S. S.; Buehler, M. J. Current Issues in Research on Structure-Property Relationships in Polymer Nanocomposites. *Polymer* **2010**, *51*, 3321−3343.

(10) Song, Y.; Zheng, Q. Concepts and Conflicts in Nanoparticles Reinforcement to Polymers beyond Hydrodynamics. *Prog. Mater. Sci.* **2016**, *84*, 1−58.

(11) Mujtaba, A.; Keller, M.; Ilisch, S.; Radusch, H.-J.; Thurn-Albrecht, T.; Saalwachter, K.; Beiner, M. Mechanical Properties and Cross-Link Density of Styrene-Butadiene Model Composites Containing Fillers with Bimodal Particle Size Distribution. *Macromolecules* **2012**, *45*, 6504−6515.

(12) Mujtaba, A.; Keller, M.; Ilisch, S.; Radusch, H.-J.; Beiner, M.; Thurn-Albrecht, T.; Saalwachter, K. Detection of Surface-Immoblized Components and Their Role in Viscoelastic Reinforcement of Rubber-Silica Nanocomposites. *ACS Macro Lett.* **2014**, *3*, 481−485.

(13) Stickney, P. B.; Falb, R. D. Carbon Black-Rubber Interactions and Bound Rubber. *Rubber Chem. Technol.* **1964**, *37*, 1299−1340.

(14) Harton, S. E.; Kumar, S. K.; Yang, H. C.; Koga, T.; Hicks, K.; Lee, E.; Mijovic, J.; Liu, M.; Vallery, R. S.; Gidley, D. W. Immobilized Polymer Layers on Spherical Nanoparticles. *Macromolecules* **2010**, *43*, 3415−3421.

(15) Jouault, N.; Moll, J. F.; Meng, D.; Windsor, K.; Ramcharan, S.; Kearney, C.; Kumar, S. K. Bound Polymer Layer in Nanocomposites. *ACS Macro Lett.* **2013**, *2*, 371−374.

(16) Jiang, N.; Endoh, M. K.; Koga, T.; Masui, T.; Kishimoto, H.; Nagao, M.; Satija, S. K.; Taniguchi, T. Nanostructures and Dynamics of Macromolecules Bound to Attractive Filler Surfaces. *ACS Macro Lett.* **2015**, *4*, 838−842.

(17) Baeza, G. P.; Dessi, C.; Costanzo, S.; Zhao, D.; Gong, S.; Alegria, A.; Colby, R. H.; Rubinstein, M.; Vlassopoulos, D.; Kumar, S. K. Network Dynamics in Nanofilled Polymers. *Nat. Commun.* **2016**, *7*, 11368.

(18) Griffin, P. J.; Bocharova, V.; Middleton, L. R.; Composto, R. J.; Clarke, N.; Schweizer, K. S.; Winey, K. I. Influence of the Bound Polymer Layer on Nanoparticle Diffusion in Polymer Melts. *ACS Macro Lett.* **2016**, *5*, 1141−1145.

(19) Jouault, N.; Crawford, M. K.; Chi, C.; Smalley, R. J.; Wood, B.; Jestin, J.; Melnichenko, Y. B.; He, L.; Guise, W. E.; Kumar, S. K. Polymer Chain Behavior in Polymer Nanocomposites with Attractive Interactions. *ACS Macro Lett.* **2016**, *5*, 523−527.

(20) Koga, T.; Barkley, D.; Nagao, M.; Taniguchi, T.; Carrillo, J.-M. Y.; Sumpter, B. G.; Masui, T.; Kishimoto, H.; Koga, M.; Rudick, J. G.;

Endoh, M. K. Interphase Structures and Dynamics near Nanofiller Surfaces in Polymer Solutions. *Macromolecules* **2018**, *51*, 9462−9470.
(21) Jimenez, A. M.; Zhao, D.; Misquitta, K.; Jestin, J.; Kumar, S. K. Exchange Lifetimes of the Bound Polymer Layer on Silica Nanoparticles. *ACS Macro Lett.* **2019**, *8*, 166−171.
(22) Popov, I.; Carroll, B.; Bocharova, V.; Genix, A.-C.; Cheng, S.; Khamzin, A.; Kisliuk, A.; Sokolov, A. P. Strong Reduction in Amplitude of the Interfacial Segmental Dynamics in Polymer Nanocomposites. *Macromolecules* **2020**, *53*, 4126−4135.
(23) Choi, J.; Hore, M. J. A.; Meth, J. S.; Clarke, N.; Winey, K. I.; Composto, R. J. Universal Scaling of Polymer Diffusion in Nanocomposites. *ACS Macro Lett.* **2013**, *2*, 485−490.
(24) Gam, S.; Meth, J. S.; Zane, S. G.; Chi, C.; Wood, B. A.; Winey, K. I.; Clarke, N.; Composto, R. J. Polymer Diffusion in a Polymer Nanocomposite: Effect of Nanoparticle Size and Polydispersity. *Soft Matter* **2012**, *8*, 6512−6520.
(25) Schneider, G. J.; Nusser, K.; Willner, L.; Falus, P.; Richter, D. Dynamics of Entangled Chains in Polymer Nanocomposites. *Macromolecules* **2011**, *44*, 5857−5860.
(26) Li, S.; Ding, M.; Shi, T. Spatial Distribution of Entanglements and Dynamics in Polymer Films Confined by Smooth Walls. *Polymer* **2019**, *172*, 365−371.
(27) Zhou, Y.; Yavitt, B.; Zhou, Z.; Bocharova, V.; Salatto, D.; Endoh, M.; Ribbe, A.; Sokolov, A.; Koga, T.; Schweizer, K. S. Bridging Controlled Network Microstructure and Long Wavelength Fluctuations in Silica-Poly(2-Vinylpyridine) Nanocomposites: Experimental Results and Theoretical Analysis. *Macromolecules* **2020**, *53*, 6984−6994.
(28) Tauban, M.; Delannoy, J.-Y.; Sotta, P.; Long, D. R. Effect of Filler Morphology and Distribution State on the Linear and Nonlinear Mechanical Behavior of Nanofilled Elastomers. *Macromolecules* **2017**, *50*, 6369−6384.
(29) Merabia, S.; Sotta, P.; Long, D. R. A Microscopic Model for the Reinforcement and the Nonlinear Behavior of Fllled Elastomers and Themoplastic Elastomers (Payne and Mullins Effects). *Macromolecules* **2008**, *41*, 8252−8266.
(30) Chen, Q.; Gong, S.; Moll, J.; Zhao, D.; Kumar, S. K.; Colby, R. H. Mechanical Reinforcement of Polymer Nanocomposites from Percolation of a Nanoparticle Network. *ACS Macro Lett.* **2015**, *4*, 398−402.
(31) Cheng, S.; Bocharova, V.; Belianinov, A.; Xiong, S.; Kisliuk, A.; Somnath, S.; Holt, A. P.; Ovchinnikova, O. S.; Jesse, S.; Martin, H.; Etampawala, T.; Dadmun, M.; Sokolov, A. P. Unraveling the Mechanism of Nanoscale Mechanical Reinforcement in Glassy Polymer Nanocomposites. *Nano Lett.* **2016**, *16*, 3630−3637.
(32) Koga, T.; Hashimoto, T.; Takenaka, M.; Aizawa, K.; Amino, N.; Nakamura, M.; Yamaguchi, D.; Koizumi, S. New Insight into Hierarchical Structures of Carbon Black Dispersed in Polymer Matrices: A Combined Small-Angle Scattering Study. *Macromolecules* **2008**, *41*, 453−464.
(33) Kohjiya, S.; Katoh, A.; Suda, T.; Shimanuki, J.; Ikeda, Y. Visualisation of Carbon Black Networks in Rubbery Matrix by Skeletonisation of 3D-TEM Image. *Polymer* **2006**, *47*, 3298−3301.
(34) Chambon, F.; Winter, H. H. Analysis of Linear Viscoelasticity of a Crosslinking Polymer at the Gel Point. *J. Rheol.* **1986**, *30*, 367.
(35) Sarvestani, A. S.; Picu, C. R. Network Model for the Viscoelastic Behavior of Polymer Nanocomposites. *Polymer* **2004**, *45*, 7779−7790.
(36) Chernyak, Y. B.; Leonov, A. I. On the Theory of the Adhesive Friction of Elastomers. *Wear* **1986**, *108*, 105−138.
(37) Yang, J.; Melton, M.; Sun, R.; Yang, W.; Cheng, S. Decoupling the Polymer Dynamics and the Nanoparticle Network Dynamics of Polymer Nanocomposites through Dielectric Spectroscopy and Rheology. *Macromolecules* **2020**, *53*, 302−311.
(38) Koga, T.; Li, C.; Endoh, M. K.; Koo, J.; Rafailovich, M.; Narayanan, S.; Lee, D. R.; Lurio, L. B.; Sinha, S. K. Reduced Viscosity of the Free Surface in Entangled Polymer Melt Films. *Phys. Rev. Lett.* **2010**, *104*, No. 066101.
(39) Nogales, A.; Fluerasu, A. X-Ray Photon Correlation Spectroscopy for the Study of Polymer Dynamics. *Eur. Polym. J.* **2016**, *81*, 494−504.
(40) Senses, E.; Narayanan, S.; Mao, Y.; Faraone, A. Nanoscale Particle Motion in Attractive Polymer Nanocomposites. *Phys. Rev. Lett.* **2017**, *119*, 237801.
(41) de Gennes, P. G. Liquid Dynamics and Inelastic Scattering of Neutrons. *Physica* **1959**, *25*, 825−839.
(42) Madsen, A.; Leheny, R. L.; Guo, H.; Sprung, M.; Czakkel, O. Beyond Simple Exponential Correlation Functions and Equilibrium Dynamics in X-Ray Photon Correlation Spectroscopy. *New J. Phys.* **2010**, *12*, No. 055001.
(43) Cipelletti, L.; Ramos, L.; Manley, S.; Pitard, E.; Weitz, D. A.; Pashkovski, E. E.; Johansson, M. Universal Non-Diffusive Slow Dynamics in Aging Soft Matter. *Faraday Discuss.* **2003**, *123*, 237−251.
(44) Bengtzelius, U.; Gotze, W.; Sjolander, A. Dynamics of Supercooled Liquids and the Glass Transition. *J. Phys. C: Solid State Phys.* **1984**, *17*, 5915−5934.
(45) Reichman, D. R.; Charbonneau, P. Mode-Coupling Theory. *J. Stat. Mech.: Theory Exp.* **2005**, *2005*, P05013.
(46) Fuchs, M. MCT Results for a Simple Liquid at the Glass Transition. *Transp. Theory Stat. Phys.* **1995**, *24*, 855−880.
(47) Cohen, E. G. D.; Verberg, R.; Schepper, I. M. D. Viscosity and Diffusion in Hard-Sphere-Like Colloidal Suspensions. *Phys. A* **1998**, *251*, 251−265.
(48) Hall, L. M.; Schweizer, K. S. Many Body Effects on the Phase Separation and Structure of Dense Polymer-Particle Melts. *J. Chem. Phys.* **2008**, *128*, 234901.
(49) Flenner, E.; Szamel, G. Relaxation in a Glassy Binary Mixture: Comparison of the Mode-Coupling Theory to a Brownian Dynamics Simulation. *Phys. Rev. E* **2005**, *72*, No. 031508.
(50) Sköld, K. Small Energy Transfer Scattering of Cold Neutrons from Liquid Argon. *Phys. Rev. Lett.* **1967**, *19*, 1023−1025.
(51) Medina-Noyola, M. Long-Time Self-Diffusion in Concentrated Colloidal Dispersions. *Phys. Rev. Lett.* **1988**, *60*, 2705−2708.
(52) Sobolev, O. De Gennes Narrowing and Hard-Sphere Approach. *J. Phys. Chem. B* **2016**, *120*, 9969−9977.
(53) Tung, W.-S.; Griffin, P. J.; Meth, J. S.; Clarke, N.; Composto, R. J.; Winey, K. I. Temperature-Dependent Suppression of Polymer Diffusion in Polymer Nanocomposites. *ACS Macro Lett.* **2016**, *5*, 735−739.
(54) Doi, M.; Edwards, S. F. *The Theory of Polymer Dynamics*; Clarendon Press: Oxford, 1986.
(55) Li, Y.; Kröger, M.; Liu, W. K. Dynamic Structure of Unentangled Polymer Chains in the Vicinity of Non-Attractive Nanoparticles. *Soft Matter* **2014**, *10*, 1723−1737.
(56) Yamamoto, U.; Schweizer, K. S. Theory of Nanoparticle Diffusion in Unentangled and Entangled Polymer Melts. *J. Chem. Phys.* **2011**, *135*, 224902−224902.
(57) Yamamoto, U.; Schweizer, K. S. Theory of Entanglements and Tube Confinement in Rod−Sphere Nanocomposites. *ACS Macro Lett.* **2013**, *2*, 955−959.
(58) Cai, L.-H.; Panyukov, S.; Rubinstein, M. Mobility of Nonsticky Nanoparticles in Polymer Liquids. *Macromolecules* **2011**, *44*, 7853−7863.
(59) Divandari, M.; Morgese, G.; Trachsel, L.; Romio, M.; Dehghani, E. S.; Rosenboom, J.-G.; Paradisi, C.; Zenobi-Wong, M.; Ramakrishna, S. N.; Benetti, E. M. Topology Effects on the Structural and Physicochemical Properties of Polymer Brushes. *Macromolecules* **2017**, *50*, 7760−7769.
(60) Payne, A. R. Dynamic Properties of Heat-Treated Butyl Vulcanizates. *J. Appl. Polym. Sci.* **1963**, *7*, 873−885.
(61) Merabia, S.; Sotta, P.; Long, D. R. Unique Plastic and Recovery Behavior of Nanofilled Elastomers and Thermoplastic Elastomers (Payne and Mullins Effects). *J. Polym. Sci., Part B: Polym. Phys.* **2010**, *48*, 1495−1508.
(62) Rogers, M. C.; Chen, K.; Andrzejewski, L.; Narayanan, S.; Ramakrishnan, S.; Leheny, R. L.; Harden, J. L. Echoes in X-Ray

https://doi.org/10.1021/acsnano.1c01283
ACS Nano 2021, 15, 11501−11513

Speckles Track Nanometer-Scale Plastic Events in Colloidal Gels under Shear. *Phys. Rev. E* **2014**, *90*, No. 062310.
(63) Iijima, M.; Kamiya, H. Layer-by-Layer Surface Modification of Functional Nanoparticles for Dispersion in Organic Solvents. *Langmuir* **2010**, *26*, 17943−17948.

https://doi.org/10.1021/acsnano.1c01283
ACS Nano 2021, 15, 11501−11513